Planck's-constant dependence of the scaling of localization length in quantum dynamics

G. O. Morrow and L. E. Reichl
Center for Studies in Statistical Mechanics and Complex Systems, The University of Texas at Austin, Austin, Texas 78712
(Received 25 November 1997)

We demonstrate numerically that the momentum-space localization length (or more precisely its inverse, the momentum-space decay rate) for a quantum system experiencing nonlinear resonance exhibits scaling behavior as Planck's constant is varied. The behavior of the scaling multiplier appears to be a result of the different levels of complexity accessible to systems with different $\hbar$ values. [S1063-651X(98)00205-0]

PACS number(s): 05.45.+b, 03.65.Ge, 32.80.Wr, 32.90.+a

I. INTRODUCTION

The phase space of classical Hamiltonian systems near integrability is dominated by Kolmogorov-Arnold-Moser (KAM) tori and their broken remnants, cantori [1]. There is now strong evidence that KAM tori and cantori can play a significant role in the quantum dynamics of these systems as well [2–8]. In previous work [8], we showed (for the quantum driven rotor) that the rate of exponential decay of the momentum-space probability exhibits scaling behavior, in a region dominated by self-similar higher-order resonances, consistent with the predictions of a quantum renormalization map [1,8,9]. In the current paper we extend this result by studying the variation of the scaling properties of the momentum-space decay rate with changing Planck's constant.

II. DYNAMICAL MODEL

The classical version of the driven quantum system that we considered in [8] is governed by a Hamiltonian

$$H' = \frac{J^2}{2I} + U_a \cos(q - \Omega\tau) + U_b \cos(3q - \Omega\tau), \qquad (1)$$

where J is the angular momentum of the rotor, I is the moment of inertia, U_a and U_b are the amplitudes of the cosine potential waves, and q is the angle of the rotor. We will rescale the angular momentum in units of Planck's constant $\hbar$ so that $J = \hbar p$. If we also rescale the time as $\tau = 2It/\hbar$, the amplitudes as $U_i = \hbar^2 V_i/2I$, the frequency as $\Omega = \hbar\omega/2I$, and the Hamiltonian as $H' = H(\hbar^2/2I)$, we obtain

$$H = p^2 + V_a \cos(q - \omega t) + V_b \cos(3q - \omega t). \qquad (2)$$

The Schrödinger equation is then given by

$$i\frac{\partial}{\partial t}\psi(q,t) = \left[-\frac{\partial^2}{\partial q^2} + V_a \cos(q - \omega t) + V_b \cos(3q - \omega t) \right] \psi(q,t). \qquad (3)$$

A strobe plot of the classical phase space for $V_b = 60$, $V_a = 180$, and $\omega = 240$ is shown in Fig. 1. The pendulumlike primary resonances from the two cosine waves are obvious as are higher-order island chains.

It is useful to consider the projection of a resonance structure onto the momentum axis. For example, in Fig. 1 the projection of the period-four resonance structure is the interval $p \approx [55,66]$. The projections of cantori and KAM tori are typically intervals also. A crucial part of our argument is the observation [8] that the momentum-space decay rate of the time-averaged probability is essentially constant on each resonance projection. Consider Fig. 2, which shows a logarithmic plot of a time-averaged momentum-space probability distribution. It is obtained in the following way. We start the system in an eigenstate of the angular momentum at the center of the primary three-island resonance. We integrate the Schrodinger equation for a long time (many periods $T = 2\pi/\omega$). The probability amplitude spreads and settles into a long-time distribution. We then take a time average of this distribution to remove spurious fluctuations.

The dashed lines in Fig. 2 indicate the boundaries of the momentum projection of the period-four resonance structure. Between the line $p = 55$ and the one at $p = 66$, $\ln P(p)$ is a linear function of p. The wave function's decay remains es-

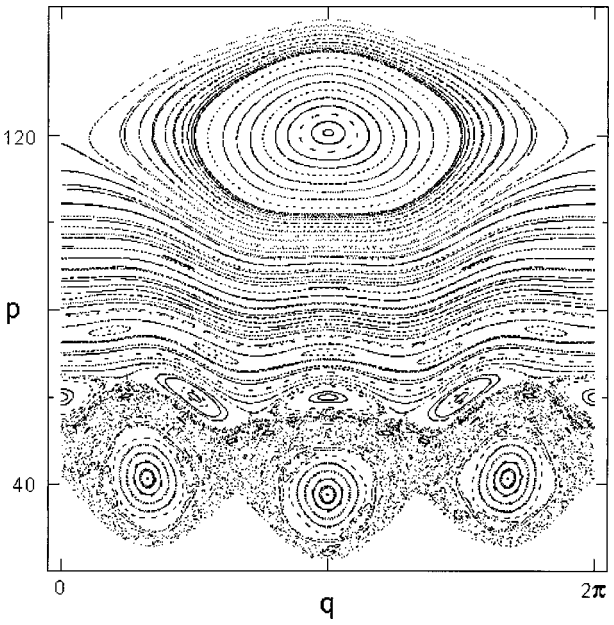

FIG. 1. Strobe plot of the classical phase space. The parameter values are $V_a = 180$, $V_b = 60$, and $\omega = 120$.

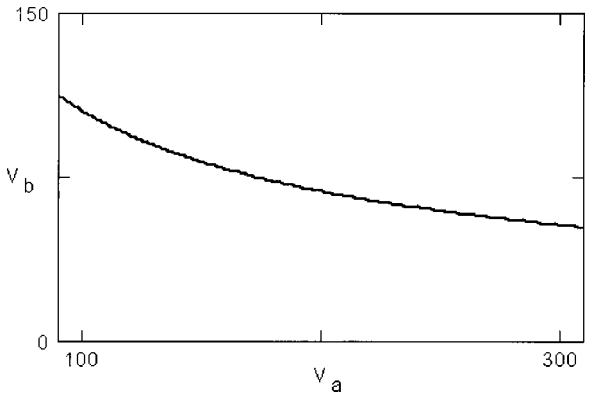

FIG. 2. Part of the stable manifold of the golden mean torus. The manifold is computed by direct iteration of the renormalization map.

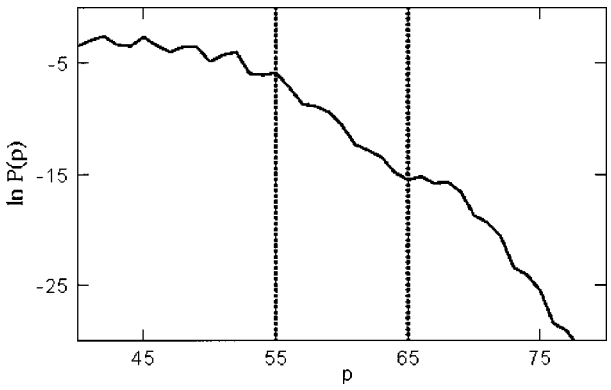

FIG. 3. Logarithmic plot of the time-averaged momentum-space probability distribution for the parameters $V_a=160$, $V_b=35$, and $\omega=120$. The dotted lines delimit the projection of the classical period-four resonance.

sentially exponential to the right of the period-four region, but with different decay rate. Within the period-four projection, the probability behaves as $P(p)\sim e^{-\lambda(p-p_0)}$, where p_0 is the left end of the projection of the classical period-four structure.

As discussed at great length in [8], if we vary the parameters V_a or V_b for a particular value of frequency ω, we can compute the variation of the momentum-space decay rate λ as a function of these parameters. For a particular set of parameter values (V_a,V_b) we compute the time-averaged momentum-space probability. We isolate a particular region of momentum space defined as the momentum projection of the classical phase-space structure associated with a particular torus. We then compute the least-squares fit to $\ln[P(p)]$ in that region. The slope of the linear fit gives the momentum-space decay rate λ.

III. RENORMALIZATION MAP

The renormalization map for this quantum model is the basis upon which we measure scaling in this quantum system. It has been discussed in several previous references [1,8,9], so we will only summarize key results here. The renormalization map generates sequences of pairs of higher-order resonances on ever smaller scales in the Hilbert space. The map acts on dimensionless quantities $X=(2m/\omega)\sqrt{2V_a}$ and $Y=(2m/\omega)\sqrt{2V_b}$ and ν, where ν is the relative wave number of a pair of neighboring resonances [in Eq. (3) $\nu=3/1$]. Notice that X and Y do not depend on $\hbar$ since $\omega\propto\hbar^{-1}$ and $V_i\propto\hbar^{-2}$. The form of the map is

$$\nu_{i+1}=\nu_{i+1}(\nu_i),\quad X_{i+1}=X_{i+1}(X_i,Y_i,\nu_i),$$

$$Y_{i+1}=Y_{i+1}(X_i,Y_i,\nu_i), \tag{4}$$

where ν_{i+1}, X_{i+1}, and Y_{I+1} are nonlinear functions of ν_i, X_i, and Y_i.

In the classical system, the most robust KAM tori are the noble tori. The sequence of resonances that approximate these tori are the slowest to overlap as we go to smaller scales in phase space. A similar phenomenon happens in the quantum system. The quantum nonlinear resonances associated with the noble sequences of relative wave numbers are the slowest to overlap and share probability, as we go to small scales in the Hilbert space. In [8] we found that the most robust sequence of resonances in the period-four projection ($55<p<66$ in the classical plot of Fig. 1), where those whose relative wave numbers approach the golden mean $(\sqrt{5}+1)/2$.

If we restrict consideration to the golden mean torus, the renormalization is particularly simple. In this case, we can paint a fairly complete picture of the behavior of this torus solely from the renormaliztion. The renormalization map has three fixed points [8]. The fixed points at infinity and zero are attracting and the domains of attraction are separated by a codimension-1 surface, called the stable manifold, which passes through the third fixed point. The third fixed point has two stable eigenvectors and one unstable eigenvector and the stable manifold is tangential to the plane spanned by the two stable eigenvectors. The stable manifold can be computed by direct iteration of the renormalization map. Figure 3 shows part of the stable manifold (computed numerically) for the most robust sequence of resonance pairs, namely, those approximating the golden mean torus. All the resonances in the sequences associated with these limiting relative wave numbers fall between the period-four and period-three resonances.

If the renormalization map acts on a function $Q(Z)$ of parameter $Z=(X,Y)$, then the function $Q(Z)$ is said to scale under the renormalization if $T\circ Q(Z)\equiv Q(TZ)=\chi Q(Z)$, where T is the renormalization transformation and χ is a real constant that only depends on the function Q. In the case of such an observable, it can be shown [8] that $Q(Z)\propto|Z-Z^*|^{\ln\chi/\ln\delta}$, where δ is the unstable eigenvalue of the renormalization map and $|Z-Z^*|$ is the distance in parameter space of the point Z from the stable manifold, measured along the unstable direction. This equation provides part of the underpinning of our numerical signature of scaling in the quantum model.

For a particular value of the driving frequency ω, we fix V_a at V_a^0 and then compute λ for several values of V_b. We then construct a plot of $\ln(\lambda)$ versus $\ln(|V_b-V^*|)$, where V^* is the intersection of the vertical line $V_a=V_a^0$ with the stable manifold of the golden mean torus. Figure 4 shows one such plot for the case $\omega=1600$. The error bars are derived from the least-squares fit to the momentum-space probability. The line shown is the least-squares fit to these points. The funda-

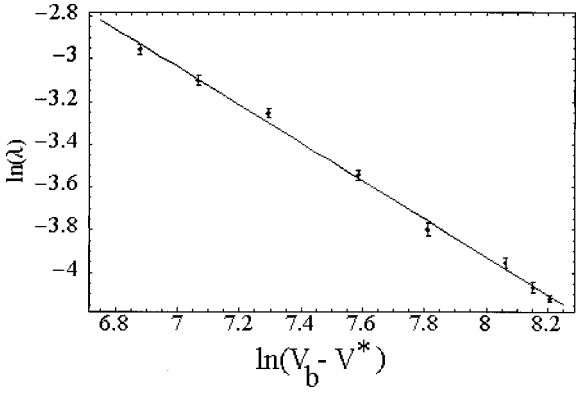

FIG. 4. Plot of the scaling relation for the momentum-space decay rate in the period-four projection. The parameters are $\omega = 1600$, $V_a = 54\,496$, and $V_b = 8000$, 8200, 8500, 9000, 9500, 10 200, 10 500, and 10 700. The golden mean torus's critical value along the line $V_a = 54\,496$ is $V^* = 7986$. The error bars are derived from the least-squares fit to the momentum-space probability.

mentally important result is that there exists a scaling relation for this quantity. That is, the fact that the plot of $\ln(\lambda)$ versus $\ln(|V_b - V^*|)$ forms a straight line shows that there is a scale invariance present in this system.

From the slope of the curve in Fig. 4, we can determine the scaling parameter χ, given our knowledge of the unstable eigenvalue δ from the renormalization map. For the golden mean unstable manifold $\delta = 1.618$. This appears to be the dominant unstable manifold in the region. The slope is approximately 0.86. Since the slope is equal to $\ln \chi / \ln \delta$, we find for the scaling parameter $\chi \approx 0.65 \pm 0.02$.

IV. VARIATION OF THE SCALING MULTIPLIER WITH $\hbar$

The preceding section displays the scaling relation for fixed $\omega = 1600$ (and therefore for a fixed $\hbar$), but variable amplitudes V_a and V_b. In this section we wish to look at the effect of changing $\hbar$. We consider a point (X_0, Y_0) near the golden mean stable manifold, in the renormalization space. We then vary $\hbar$ by varying both ω and V_a, V_b so that (X_0, Y_0) remains fixed. We also scale the momentum by ω so $\tilde{p} = p/\omega$. (The momentum scaling serves to map corresponding phase-space structures to a single momentum value for all the different $\hbar$ values.) The values of ω we considered form the sequence

$$\omega = 100, 120, 200, 400, 800, 1600. \tag{5}$$

In Fig. 5 we show our results for the slope of the scaling relation curve versus $\hbar$. Because we have scaled $\hbar$ out of our equations of motion, the value of ω fixes $\hbar$, up to an overall normalization (recall that $\omega \propto \hbar^{-1}$). To plot the slope versus $\hbar$ relation we have simply taken $\hbar = \omega^{-1}$. The slope of the scaling relation appears to decrease and may be approaching a limiting value as $\hbar$ becomes very small (the classical result in Sec. V gives a limiting value).

The range of our calculation is naturally limited by two factors. First, it is difficult to obtain reliable results for very large $\hbar$ (i.e., very quantum systems) because the time-averaged momentum-space probability in these cases is very

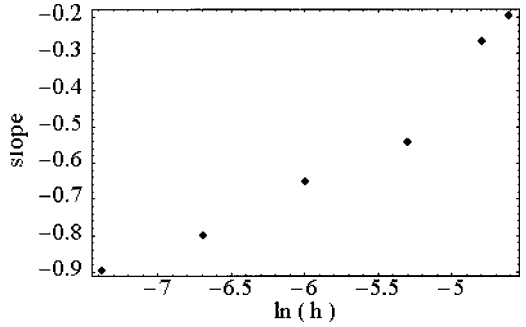

FIG. 5. Slopes of the scaling relation curves plotted versus the logarithm of Planck's constant. Each slope is derived from a least-squares fit to the scaling relation.

oscillatory on the scale on which we wish to approximate it as linear. Second, on the side of small $\hbar$, the numerical simulations become more and more expensive in computer resources, as we must include a greater and greater number of basis states to model the system. Our data represent a compromise between these two factors.

V. SCALING IN THE CLASSICAL MODEL

Although our numerical simulations of the quantum system are limited in their approach to the semiclassical limit (because of computer resources, see the discussion above), we can perform the analysis on the fully classical system rather cheaply. In order to compute a quantity similar to the quantum momentum-space probability for the classical model, we begin with an ensemble that is similar to the initial quantum state. The initial quantum state was a momentum eigenstate $|m\rangle$. The position representation of such a state is $\psi(x,0) = \langle x|m\rangle = e^{imx}/\sqrt{2\pi}$, so the initial probability is uniform in the position direction. We begin our classical simulation with an ensemble localized in momentum and uniform in position.

We propagate the ensemble forward by a large number of field periods (in our case 600 field periods) and then we plot the points in the ensemble at $t = 600T$. This plot is shown in Fig. 6. Next we divide the momentum axis into bins and count the number of trajectories that lie in each bin. A logarithimic plot of bin counts is shown in Fig. 7(a). We can carry out the same scaling analysis on the classical data as we did on the quantum data. We simply create a picture like Fig. 7(a) for several different nonlinearity parameters, find

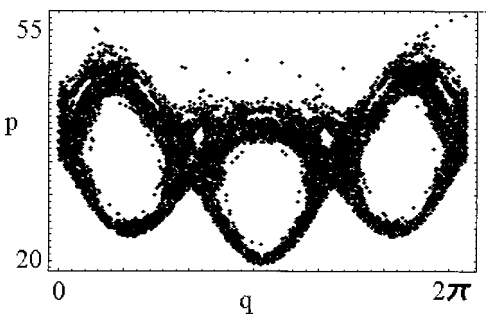

FIG. 6. Progress of an initially localized classical ensemble after 600 field periods. The parameters are $\omega = 100$, $V_a = 210$, and $V_b = 31$. There are 10^5 points in the ensemble.

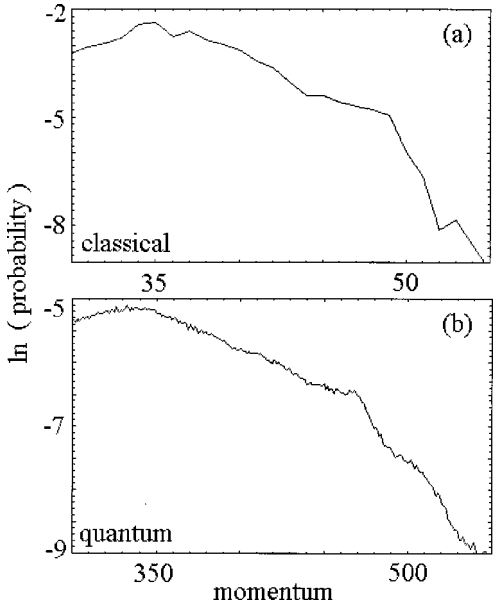

FIG. 7. Logarithmic plot of the (a) classical and (b) quantum probabilities. The parameters are $\omega=100$, $V_a=210$, and $V_b=31$. There are 10^5 points in the classical ensemble. The quantum momentum axis is scaled by 10 because the ω value was 1000 for that plot.

the slopes in the relevant region, and plot the logarithm of the slopes versus the logarithm of $|V_b-V^*|$. The scaling data are shown in Fig. 8. The data give a value for the scaling multiplier of

$$\chi_{classical}=0.59\pm0.2. \tag{6}$$

We believe this gives a left-hand limit for the data presented in Fig. 5. It appears that the quantum data tend toward this classical value as $\hbar$ is decreased.

VI. ANALYSIS

In classical systems, the important quantity for describing transport of phase space trajectories through regions dominated by cantori is the ''cantorus flux,'' which is the rate of transport of trajectories across the broken remnants of a KAM barrier. The cantorus flux scales under the classical

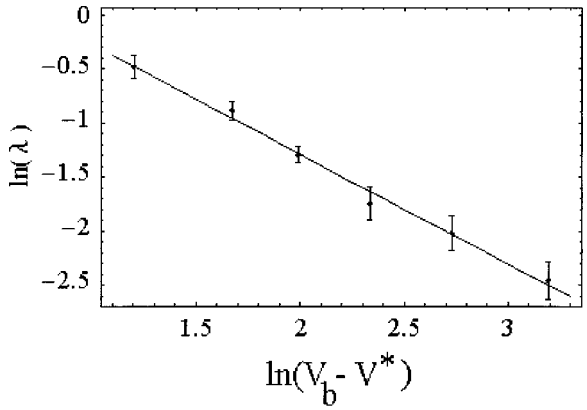

FIG. 8. Plot of the scaling relation for the classical system. The parameters are $\omega=100$, $V_a=210$, and $V_b=31$, 33, 35, 38, 43, and 52. The critical value for V_b is $V^*=27.67$.

renormalization map [4,10,11]. Numerical experiments [3,12,13] suggest that the quantum system corresponding to a classically chaotic Hamiltonian system ''feels'' the underlying classical structure. In particular, the presence of KAM tori and certain cantori in the classical phase space signals an exponential decay in the quantum momentum-space probability in the momentum region occupied by the classical structures.

The quantum system does not appear to be affected by structures in the underlying classical phase space that are smaller than $\hbar$. A classical trajectory is allowed to interact with structures of any spatial scale in the phase space, but a quantum ''trajectory'' (wave packet) is limited and only responds to phase-space structures on the order of or larger than $\hbar$ in area. We have noted a similar behavior [8] in the Floquet eigenstates of the two resonance system. The Floquet eigenstates correspond to classical phase-space structures (in, for example, the Husimi representation). However, there are no Floquet eigenstates associated with phase-space structures whose area is smaller than roughly $\hbar$.

Meiss and Ott [13] used this notion of ''accessible'' phase-space scales to obtain a scaling relation for the quantum-classical crossover time for a system at its critical nonlinearity parameter. Lai, Ott, and Grebogi [14] extended the result to noncritical parameter values. Note that in both cases, the authors derive a scaling relation, but do not derive values for the scaling parameters.

VII. SCALING MULTIPLIER'S DEPENDENCE ON $\hbar$

We now discuss how the idea of accessible phase-space scales affects the renormalization. We begin with some results from the purely classical renormalization that concern the behavior of cantorus flux. As was mentioned above, the cantorus flux scales under the classical renormalization [10,11]. The idea is that there is a simple relation between the flux through successive resonance chains in the sequence of rational approximates to a particular (near-critical) torus. If we label the rational approximate chain with an index i (where $i>j$ implies that the resonance chain i has higher period than chain j, smaller phase-space area per resonance island than chain j, and closer proximity to the torus than does chain j) and if we denote the flux through the rational approximate chain i by W_i, then it has been shown [10] that

$$W_i>W_j \Leftrightarrow i<j. \tag{7}$$

Starting from the scaling relation for flux, it can be shown [10,11] that the difference in flux as the nonlinearity parameter is increased away from its critical value is proportional to the flux itself:

$$W_i(\Delta K)-W_i((\Delta K)/\delta)=W_i(\Delta K)\left(1-\frac{1}{\alpha\beta}\right). \tag{8}$$

(Here the nonlinearity parameter is represented by K, $\Delta K=K-K^*$, and α, β, and δ are positive classical scaling parameters.) We conclude that in the classical system, the change in flux under a given change in nonlinearity parameter is greater for the lower-order resonance chains (i.e., those labeled by a smaller value of i).

We now make the connection to the quantum system. We use Planck's constant as a yardstick to decide which classical phase-space structures are important in a given quantum system. We note the conjecture of Mackay, Meiss, and Percival [4] that there is a direct connection between the classical cantorus flux and the quantum momentum-space probability decay rate.

Consider quantum systems with two different values of Planck's constant $\hbar_i$ and $\hbar_j$ and let us suppose that $\hbar_i > \hbar_j$. Then the j system will interact with higher-order resonances than will the i system. From the discussion above, we then expect that for a given change in nonlinearity parameter, there will be a greater change in flux for the i system than for the j system. Therefore, we expect a greater change in the decay rate for the i system than for the j system. Given the definition of the scaling multiplier χ,

$$T \circ Q(Z) = \chi Q(Z), \tag{9}$$

and recalling that the quantum renormalization map's effect upon nonlinearity parameter $Z=(X,Y)$ is independent of Planck's constant, we conclude that $\chi_i > \chi_j$.

Let us follow this line of reasoning toward the $\hbar \to 0$ limit. As $\hbar$ gets smaller and smaller, the quantum system ''sees'' smaller and smaller scales in the phase space. Since the classical system already sees all scales, we conclude that $\chi_{classical}$ is a lower bound on the quantum values.

Figure 5 shows the slope of the λ versus $|X-X^*|$ curve plotted versus the logarithm of $\hbar$. (Note that slope is equal to $\ln \chi / \ln \delta$, where δ is the unstable eigenvalue of the renormalization.) Figure 5 shows that the slope indeed decreases with decreasing $\hbar$. Noting the value of the slope of the corresponding classical curve is ≈ -1.1, we see that it is plausible that the quantum slope smoothly approaches the classical value.

VIII. CONCLUSION

We have shown numerical evidence that the extent of the localization in momentum space (or, equivalently, the momentum-space decay rate) of a driven, continuous-time quantum Hamiltonian system exhibits a scaling behavior. In particular, the momentum-space decay rate approximately satisfies a relation of the form $\lambda \propto |z - z_c|^{\ln \chi / \ln \delta}$. This behavior is consistent with that of a ''scaling function,'' i.e., a physical function that is homogeneous under the renormalization transformation. Further, we show that the scaling multiplier χ decreases with decreasing $\hbar$. We explain this fact using arguments based on the course-grained phase space previously employed to derive scaling relations for the quantum-classical crossover time.

ACKNOWLEDGMENTS

The authors wish to thank the Robert A. Welch Foundation, Grant No. F-1051, for support of this work. We also wish to thank the University of Texas System Center for High Performance Computing and NERSC for the use of their computation facilities.

[1] L. E. Reichl, *The Transition to Chaos in Conservative Classical Systems: Quantum Manifestations* (Springer-Verlag, Berlin, 1992).
[2] G. P. Berman and G. M. Zaslavskii, Phys. Lett. **61A**, 295 (1977).
[3] R. S. MacKay and J. D. Meiss, Phys. Rev. A **37**, 4702 (1988).
[4] R. S. MacKay, J. D. Meiss, and I. C. Percival, Physica D **13**, 55 (1984).
[5] D. R. Grempel, R. E. Prange, and S. Fishman, Phys. Rev. A **29**, 1639 (1984).
[6] L. E. Reichl and W. A. Lin, Phys. Rev. A **33**, 3598 (1986).
[7] T. Geisel, G. Radons, and J. Rubner, Phys. Rev. Lett. **57**, 2883 (1986).
[8] G. O. Morrow and L. E. Reichl, Phys. Rev. A **50**, 2027 (1994).
[9] L. E. Reichl and Li Haoming, Phys. Rev. A **42**, 4543 (1990).
[10] R. S. Mackay, Ph.D. thesis, Princeton University, 1982 (unpublished).
[11] D. Bensimon and L. E. Kadanoff, Physica D **13**, 82 (1984).
[12] R. C. Brown and R. E. Wyatt, Phys. Rev. Lett. **57**, 1 (1986).
[13] J.D. Meiss and E. Ott, Physica D **20**, 387 (1986).
[14] Y. C. Lai, E. Ott, and C. Grebogi, Phys. Lett. A **173**, 148 (1993).